Available online at www.sciencedirect.com
ScienceDirect
Trans. Nonferrous Met. Soc. China 31(2021) 2687−2702
Transactions of Nonferrous Metals Society of China
www.tnmsc.cn

Comparison of explosive welding of pure titanium/SUS 304 austenitic stainless steel and pure titanium/SUS 821L1 duplex stainless steel

Xiang CHEN[1], Daisuke INAO[2], Shigeru TANAKA[1], Xiao-jie LI[3], I. A. BATAEV[4], Kazuyuki HOKAMOTO[1]

1. Institute of Industrial Nanomaterials, Kumamoto University, 860-8555 Kumamoto, Japan;
2. Faculty of Engineering, Kumamoto University, 860-8555 Kumamoto, Japan;
3. State Key Laboratory of Structural Analysis for Industrial Equipment and Department of Engineering Mechanics, Dalian University of Technology, Dalian 116024, China;
4. Faculty of Mechanical Engineering and Technologies, Novosibirsk State Technical University, K. Marks 20, 630073 Novosibirsk, Russia

Received 15 October 2020; accepted 2 March 2021

Abstract: Pure commercial titanium was welded with two types of stainless steel, namely SUS 304 austenitic stainless steel and SUS 821L1 duplex stainless steel. The wavy interface of SUS 821L1 was smaller than that of SUS 304. The vortex zone was observed from both longitudinal and transverse directions, and its composition was analyzed. The interface of Ti/SUS 821L11 was able to bear 401−431 MPa shear load while that of Ti/SUS 304 could withstand 352−387 MPa. The weldability window was used to analyze experimental phenomenon. Furthermore, the smoothed particle hydrodynamics (SPH) numerical simulation method was used to simulate the wavy interface. The trend of wavelength and amplitude change with strength and the stand-offs was consistent with the experimental results.
Key words: explosive welding; titanium; duplex stainless steel; tensile shear test; weldability window; smoothed particle hydrodynamics (SPH)

1 Introduction

Titanium and titanium alloys are widely used in the aviation, chemistry, biomedicine and nuclear industries. This is because they offer the advantages of low density, high strength, excellent resistance to corrosion and high impact toughness [1]. Structural parts of titanium or titanium alloys and stainless steel can be used in aerospace engineering, chemical and petrochemical industries, heat exchangers, nuclear reactors and nuclear fuel reprocessing [2,3]. Currently, the main methods of combining titanium/titanium alloys with stainless steel involve friction welding [4], pulsed laser welding [5], fusion welding [6], diffusion bonding [7], friction stir welding [8] and explosive welding [9]. Among them, explosive welding has the advantage of producing high-strength and large-area composite plates [10,11].

Presently, a number of studies exist on the use of explosive welding to bond titanium and stainless steel. For instance, MUDALI et al [12] welded pure titanium and AISI 304L stainless steel to study corrosion and microstructure of the joined product. Though the corrosion rate was high, it was acceptable as corrosion attack was on the stainless steel portion of the joint. Additionally, KAHRAMAN et al [13] welded titanium alloy (Ti–6Al–4V) with austenitic stainless steel using different explosive loads to compare the different morphologies of the interface. They found that the

Corresponding author: Kazuyuki HOKAMOTO, Tel: +81-963423740, E-mail: hokamoto@mech.kumamoto-u.ac.jp
DOI: 10.1016/S1003-6326(21)65685-6

welding interface was flat when using lower explosive loads, and wavy interface appeared when using higher explosive loads. Moreover, MANIKANDAN et al [14] joined pure titanium (TP 340) with SUS 304 by controlling the energy conditions to limit the generation of the melting layer at the welding interface. MOUSAVI et al [15] studied the effect of heat treatment after explosive welding on the microstructure of the interface. They showed that heat treatment promoted the formation of intermetallic phases. MOUSAVI et al [16] also joined pure titanium and AISI 304 stainless steel at different explosive loads to investigate the effect of explosive loading on the bonding interface, and brittle intermetallic phases such as Fe_2Ti, Fe_2Ti_4O and Cr_2Ti were found at the interface under high explosive loads. Although explosive welding has the advantage of preparing large-area composite plates, it is not suitable for bonding plates that are largely thick. Therefore, a recent study used an explosive welded plate as a transition joint and combined other welding methods to manufacture composite plates with large thickness. This method expanded the application of explosively welded materials [17].

In this study, the SUS 304 austenitic stainless steel and a new type of corrosion-resistant duplex stainless steel (SUS 821L1) were used. SUS 821L1 was a new kind of high strength duplex stainless steel produced by Nippon Steel Corporation in 2015 [18,19]. Compared to SUS 304, SUS 821L1 has higher strength and higher resistance to corrosion. The clad combination of duplex stainless steel and titanium has better corrosion resistance, and it can be used in highly corrosive environment. The optical microscope (OM) and scanning electron microscope (SEM) were then used to make comparisons in welding results from the two types of stainless steel. Additionally, the vortex was analyzed in the transverse direction using the electron probe microanalyzer (EPMA). The tensile shear test was also conducted to estimate the bonding strength and the fractures were analyzed. Finally, the smoothed particle hydrodynamics (SPH) method was used to simulate the process of collision between the flyer and collided plates in order to understand the mechanism of wavy interface formation.

2 Experimental

2.1 Materials

Pure commercial titanium TP 270C (JIS Grade 1), JIS SUS 304 austenite stainless steel and JIS SUS 821L1 duplex stainless steel (austenite and ferrite) were used in this study. The chemical compositions of two types of stainless steel are given in Table 1. The mechanical properties of the materials are also highlighted in Table 2. Prior to the explosive welding experiments, the hardness of the materials was measured. The hardness of welding surface of titanium is HV 145 (0.196 N loading), the hardness of thickness surface of titanium is HV 155 (0.196 N loading), the hardness of welding surface of SUS 821L1 is HV 245 (0.98 N loading), the hardness of thickness surface of SUS 821L1 is HV 300 (0.98 N loading), the hardness of welding surface of SUS 304 is HV 195 (0.98 N loading), and the hardness of thickness surface of SUS 304 is HV 310 (0.98 N loading).

Table 1 Chemical compositions of materials (wt.%) [20,21]

Material	C	H	O	N	Fe	Ti	Si	Mn	Ni	Cr
TP 270C	≤0.08	≤0.013	≤0.15	≤0.03	≤0.20	Bal.	−	−	−	−
SUS 304	≤0.08	−	−	−	Bal.	−	≤1.00	≤2.00	8.00−10.50	18.00−20.00
SUS 821L1	≤0.03	−	−	−	Bal.	−	≤0.75	2.0−4.0	1.50−2.50	20.50−21.50

Table 2 Mechanical properties of materials [20,22,23]

Material	Density/(g·cm^{-3})	Yield strength/MPa	Tensile strength/MPa	Elongation/%	Hardness (HB)
Titanium	4.54	≥165	270−410	≥27	−
SUS 304	7.90	≥205	≥520	≥40	≤200
SUS 821L1	7.80	≥400	≥600	≥25	≤290

There were clear differences in hardness between the welding and thickness interfaces due to variations in their microstructures, as shown in Fig. 1.

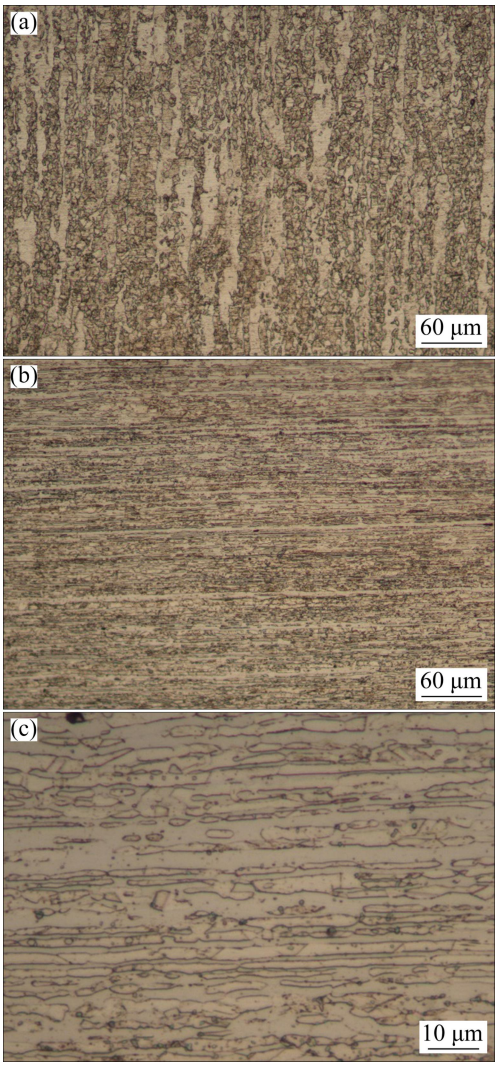

Fig. 1 Microstructures of SUS 821L1: (a) Welding interface; (b) Thickness interface; (c) Local area of (b)

2.2 Explosive welding

The main explosive used in the experiment was ANFO-A (a mixture of ammonium nitrate and fuel oil) with a density of ~530 kg/m^3. Initiation was conducted using a high detonation velocity explosive named SEP and the explosive welding configuration is shown in Fig. 2. The thickness of explosives used in the study was 48 mm. Additionally, the dimensions of the titanium and stainless steel plates were 200 mm (length) × 100 mm (width) × 3 mm (height) while those of mild steel were 260 mm (length) × 140 mm (width) × 60 mm (height). The gaps between titanium and stainless steels were set at 5, 10 and 15 mm, respectively. The parameters were selected according to Manikandan's work [9].

3 Results and discussion

3.1 Calculation of explosive welding parameters

Flyer plate velocity in the vertical direction (V_P) and the collision angle (β) are important factors in calculating the welding parameters of explosives. The relationship can be expressed using the following equation [24]:

$$V_p = 2V_D \sin(\beta/2) \tag{1}$$

where V_D is the detonation velocity of the explosive.

The collision angle β can be calculated using the following equation [25]:

$$\beta = \left(\sqrt{\frac{K+1}{K-1}} - 1\right)\frac{\pi}{2}\frac{r}{r+2.71+\dfrac{0.184t_e}{s}} \tag{2}$$

where r represents the loading ratio (mass of

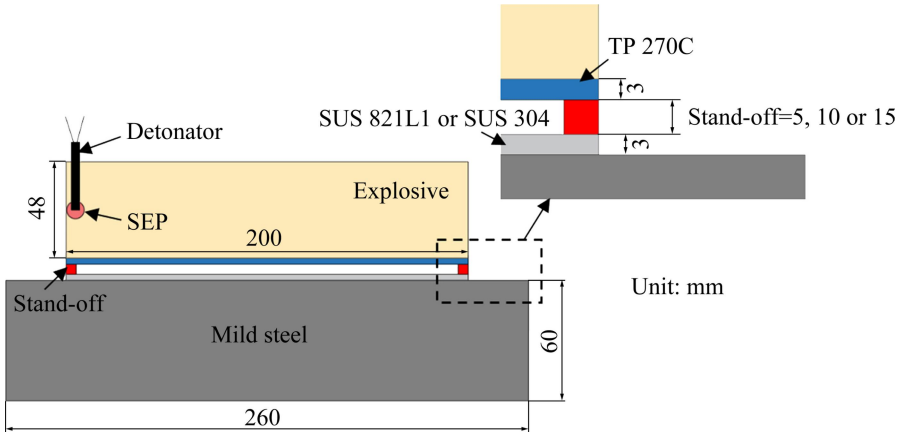

Fig. 2 Schematic of explosive welding configuration

explosive per unit mass of flyer plate), t_e and s are the explosive thickness and the stand-off distance, respectively, and K is the gaseous polytropic index of the detonation products.

Energy dissipated at the interface during the collision is crucial for the results of explosive welding. Therefore, loss of kinetic energy (ΔE_k) at collision can be calculated using the following equation [26]:

$$\Delta E_k = \frac{m_D m_C V_P^2}{2(m_D + m_C)} \quad (3)$$

where m_C is the mass per unit area of the collided plate, and m_D is the mass per unit area of the flyer plate. The calculated results are summarized in Table 3. References [9,26] give the parameters of K and V_D in Table 3.

3.2 Microstructural analysis

3.2.1 Wavelength and amplitude

Figure 3 shows that there was a wavy interface with periodic changes at the welding interface and this is the most significant feature of explosive

Table 3 Calculated flyer plate velocity V_P, collision angle β and kinetic energy loss ΔE_k

Sample No.	Gaseous polytropic index, K	Explosive ratio, r	Detonation velocity, D/(m·s^{-1})	Flying plate velocity, V_P/(m·s^{-1})	Collision angle, β/(°)	ΔE_k/(kJ·m^{-2})
1	2.48	1.87	2575	633	14.1	2053
2	2.48	1.87	2575	633	14.1	2053
3	2.48	1.87	2575	735	16.4	2766
4	2.48	1.87	2575	735	16.4	2766
5	2.48	1.87	2575	777	17.4	3088
6	2.48	1.87	2575	777	17.4	3088

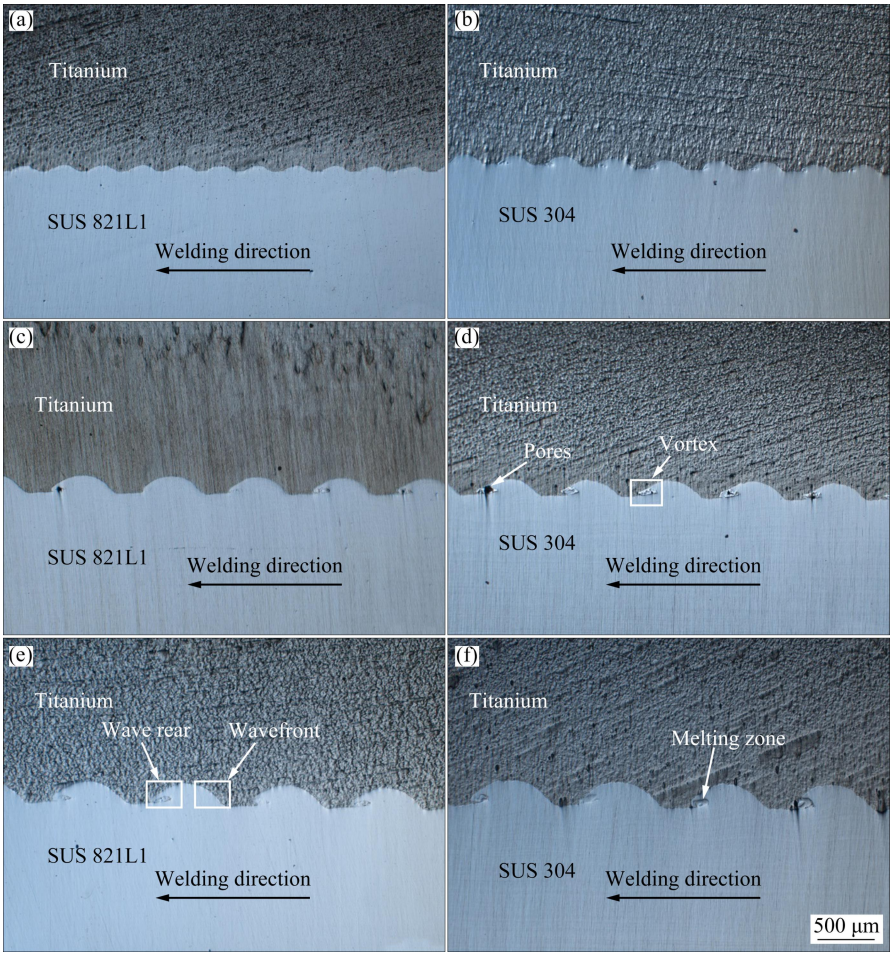

Fig. 3 Optical microscopic photographs of welding interface: (a) Sample 1; (b) Sample 2; (c) Sample 3; (d) Sample 4; (e) Sample 5; (f) Sample 6

welding [27,28]. The micro morphology of the vortex zone was slightly different in each wave although the overall wavelength and amplitude were stable. In addition, the wave was divided into the wave front and rear sections, based on the welding direction. Figure 3 and Table 3 show that an increase in stand-offs, flyer plate velocity and collision angle resulted in more loss in kinetic energy as well as an increase in both wavelength and amplitude. The relationship between kinetic energy loss and flyer plate velocity is given in Eq. (3). Whether the increase in wavelength and amplitude was related to increased flying plate velocity or increased collision angle is not clear. The welding results of SUS 821L1 and SUS 304 showed that the harder the welding surface became, the lower the wavelength and amplitude were at the interface, consistent with previous research [29], while the vortex zone at the wave rear became smaller. Under high pressure, the metals entered fluid state, and the ratio of pressure to tensile strength of Ti/SUS 304 was higher than that of Ti/SUS 821L1. When the ratio was higher, more jet would generate, and then larger wavelength and amplitude would be formed. Besides, cavities and melting areas were found in the vortex zones. Therefore, based on the experimental findings, good welding results were achieved from the three selected parameters.

3.2.2 Microstructure of interface

SUS 821L1 and pure titanium were etched using a solution containing HF (3 mL), HNO_3 (6 mL), and H_2O (91 mL). On the other hand, SUS 304 was etched using a solution containing HNO_3 (5 mL) and HCl (15 mL). Adiabatic shear is the dynamic mechanical behavior of materials under impact load, and occurs due to the heat generated from large plastic distortion in local areas, within a short time. Deformation in these areas is intensified by the generated heat. Generally, adiabatic shear can be divided into two types: one is the deformation band, characterized by a highly concentrated shear strain, sharp grain elongation and grain fragmentation; the other is the transformation band, characterized by phase transformation or grain recrystallization [30]. The adiabatic shear band (ASB) is often observed in explosively welded material due to the large plastic deformation at the interface [29,31] and the high strain rate ($>10^6$ s^{-1}) [24]. Moreover, the heat generated by large plastic deformation is usually released gradually, hence making the deformation more severe. Occasionally, adiabatic shear develops cracks. The ASB was found at the welding interface, as shown in Fig. 4. Compared to the original distribution of grains in Fig. 1(c), the grains around the ASB in Fig. 4(c) were clearly elongated and crushed, indicating that it belonged to the deformation band category. The recrystallized grains in Fig. 4(d) resulted from large plastic deformation. Moreover, an increase in plastic deformation gave rise to more cracks in the ASB, as shown in Fig. 4(f).

A metal jet is often generated during the process of explosive welding [32] and it plays a role in self-cleaning by removing oxides and portions of metal on the surface [24]. The jet assembles these materials into the vortex zone and the molten metal inside reacts to produce intermetallic compounds [33]. The vortex zone has a high cooling rate of 10^7−10^9 K/s [34], which results in the formation of amorphous alloys [35]. Therefore, the vortex zone contains a mixture of original metals, intermetallic compounds, amorphous compounds and oxides. Figures 4(e, g) show that the grains of stainless steel were obviously elongated and fragments of titanium and stainless steel were present in the vortex. Moreover, the cracks in Fig. 4(h) were caused by thermal stress during solidification [36]. The ASB occurred near the crest of the wave in SUS 304, as shown in Figs. 4(i), while in SUS 821L1 ASB spread across the wave, as indicated in Figs. 4(b, f).

In this study, the transverse section was explored in order to further understand the entire interface. The cross section of the vortex zone in the transverse direction is shown in Fig. 4(j). Stainless steel chipping and alloy phases were observed in the vortex zone. Additionally, cracks were present in both the longitudinal and transverse zones of the vortex.

3.2.3 EPMA results

Figure 5 shows the cross section of the vortex region in the transverse direction. The EPMA test results revealed that the main components in the analyzed zone were Ti, Cr, Fe, Ti+Cr, Ti+Fe, and Cr+Fe. The areas containing Cr+Fe and Fe mainly belonged to SUS 821L1. Based on the distribution of elements, it was deduced that the melting zone contained titanium, chromium, iron, an alloy phase

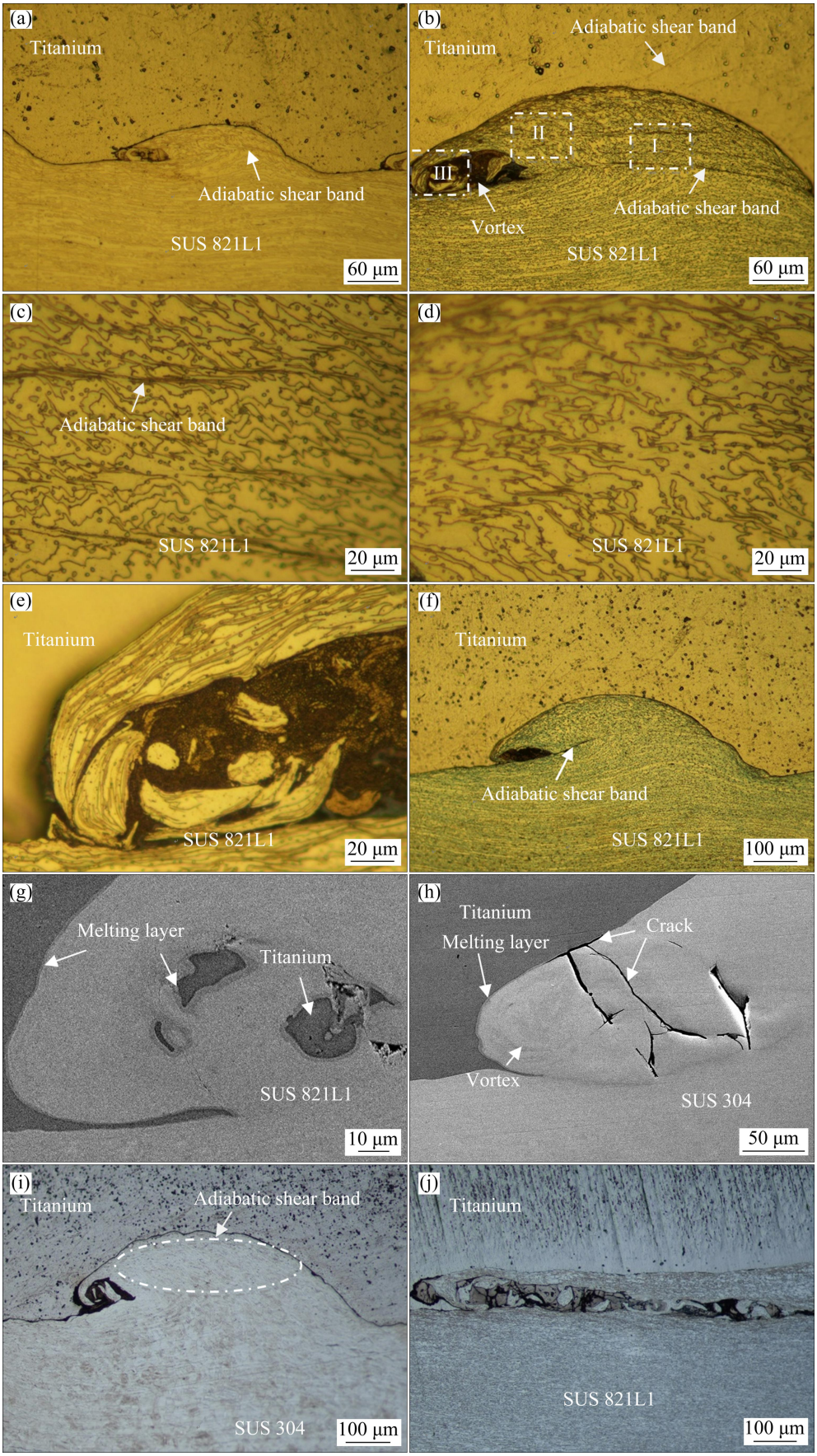

Fig. 4 Microstructures of interface: (a) Sample 1; (b) Sample 3; (c) Region I of Sample 3; (d) Region II of Sample 3; (e) Region III of Sample 3; (f) Sample 5; (g, h) Vortex zones; (i) Sample 6; (j) Transverse microstructure of vortex zone

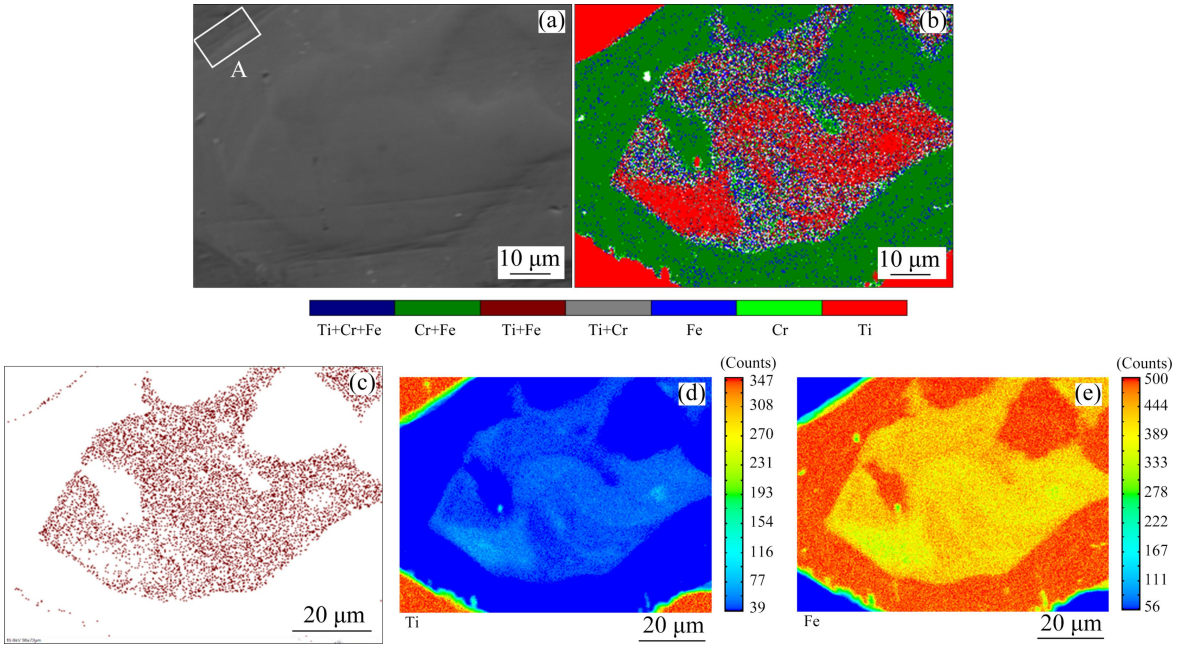

Fig. 5 EPMA results for Sample 3 in transverse direction: (a) Detection area; (b) Distribution of elements; (c) Areas containing Fe+Ti; (d) Ti element; (e) Fe element

composed of Ti and Cr, an alloy phase containing Ti and Fe, and SUS 821L1 (Cr+Fe and Fe). In Ref. [16], MOUSAVI and SARTANGI found Fe_2Ti and Cr_2Ti in the melting zone. By combining the results in Fig. 5, it can be deduced that the components of the melting zone included titanium (Ti), chromium (Cr), iron (Fe), Fe_2Ti (Ti+Fe), Cr_2Ti (Ti+Cr) and SUS 821L1 (Ti+Cr and Fe). Besides, oxides and amorphous alloys were in the melting zone [35]. The composition of the vortex region was complex, and it was mainly composed of titanium, stainless steel and Ti−Fe alloy phases. Notably, there was an alloy layer between titanium and stainless steel in Zone A, where the diffusion of elements took place.

3.3 Mechanical properties

3.3.1 Vickers hardness

The Vickers hardness test results are shown in Fig. 6. A load of 0.98 N was used to measure the hardness of stainless steel while 0.196 N was used for titanium. The first point of measurement was taken 20 μm from the interface and the subsequent measurements were made at 50 μm intervals, as indicated in Fig. 6(a). The black horizontal lines show the initial Vickers hardness values of the surface of the received materials. The hardness of the materials increased after explosive welding, due to the work-hardening. However, the hardness of titanium decreased slightly near the interface and around the vortex zone, maybe due to the heat generated in the vortex zone during welding. During the formation of the vortex zone, the materials rotate at a high speed [34] and the centrifugal force gives rise to holes or a porous structure. In Section 3.2.2, it was mentioned that the vortex region consists of a mixture of alloys, titanium, stainless steel, amorphous and oxides. Therefore, due to the influence of these factors, the hardness values in the vortex region were not uniform. Loading of 19.6 N was used to measure the mechanical properties of ASB, and the result in Fig. 6(d) showed that there were no cracks generated in the ASB under the loading. This means that the ASB in Sample 5 has a good mechanical property.

3.3.2 Tensile shear test results

Measuring the bonding strength of welded plates is rather challenging. Although the Ram tensile test is a good method of measuring the bonding strength, it has some limitations. For example, the material needs reasonable thickness and strength [26]. In addition, the ASTM side shear test was used to evaluate the bond strength. However, given that the interface of explosively welded materials was not flat, manufacturing the shear sample became difficult [37]. Moreover,

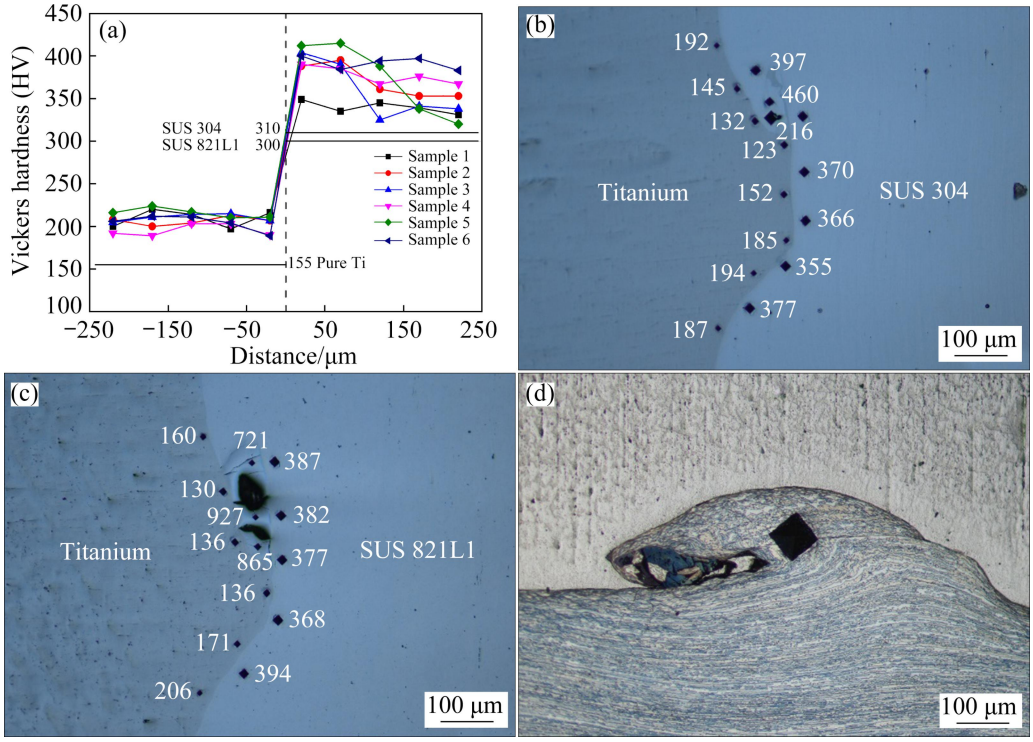

Fig. 6 Vickers hardness test results: (a) Hardness across wavy interface; (b) Sample 2; (c) Sample 5; (d) Indentation test of Sample 5

measuring the shear strength. However, they only reported the strength values, but details of the samples after testing were not availed. In this study, a method similar to that used by SHIRAN et al [38] was utilized to measure the bonding strength. The tensile shear test sample in Fig. 7(b) was taken from the processing area in Fig. 7(a). When Samples 3 and 5 were cut with a sawing machine, the welded plates were separated near the edge of the plate, which means that these areas were not well welded. In order to get a properly welded sample for the tensile shear test, the samples were manufactured by using a 0.3 mm tungsten wire and the processed area is shown in Fig. 7(a). The processed sample is shown in Fig. 7(b). Figure 7(c) clearly shows the position relationship between the cuts and interface. Additionally, the machining accuracy was crucial in ensuring that the notch was just near the interface. This corroborated with the report by DERIKVAND and PANGH [39] on making a tensile shear test sample. The loading speed was 0.1 mm/min. The test results in Table 4 show that the interface of Ti/SUS 821L11 could bear 401−431 MPa shear load while that of Ti/SUS 304 was able to withstand 352−387 MPa. The fractures are shown in Figs. 7(d−g). Figure 8 shows that the fractures of Samples 1−4 mainly occurred on the titanium side, suggesting that the bonding strength of Ti/SUS 821L1 was higher than the measured value. However, the fractures of Samples 5 and 6 occurred on both the titanium side and vortex zone. This may be attributed to the alloy layer between the vortex zone and titanium, as shown in Figs. 4(g, h). Figures 8(g−i) show that the fractures were brittle and the failure mode was slip shear. Figure 8(i) also shows several cracks in the morphology of the vortex zone. The fracture did not develop along the adiabatic shear line in duplex stainless steel, suggesting that the adiabatic shear was not obvious in this case, and it did not affect the shear strength of the interface. However, as an internal defect, the adiabatic shear line should be minimized or avoided during welding.

3.4 Weldability window

WITTMAN [40] and DERIBAS et al [41] introduced the concept of the weldability window for explosive welding. The concept takes into account the collision point velocity in the horizontal direction (V_C) and the collision angle (β). When the parameters used are within the weldability window, moderate welding results can be achieved.

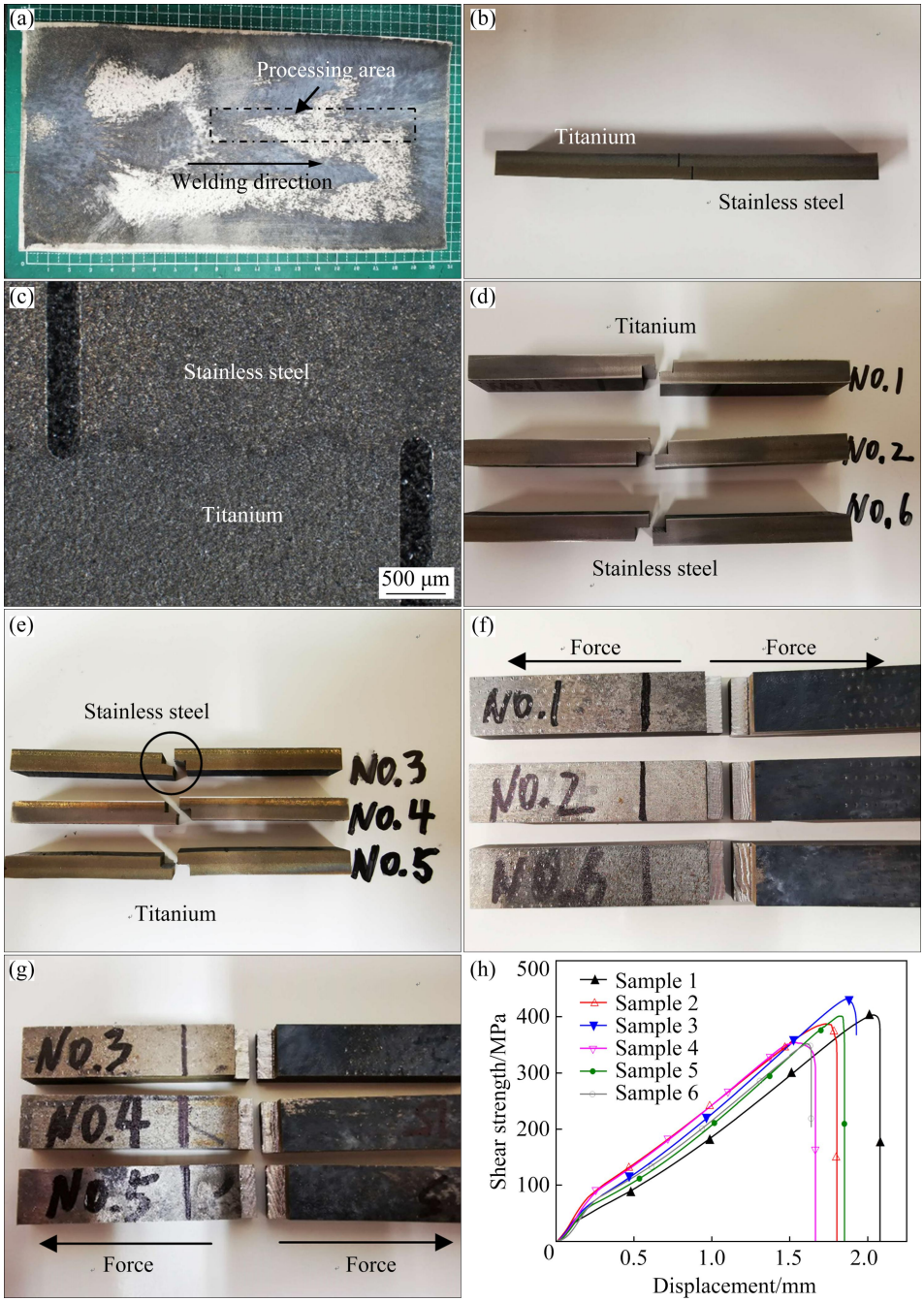

Fig. 7 Tensile shear test results: (a) Processing area; (b) Tensile shear test sample; (c) Optical microscope image for Sample 6; (d−g) Samples after testing; (h) Tensile curves

Table 4 Tensile shear test parameters

Sample No.	Length/ mm	Width/ mm	Height/ mm	Distance set between two cuts/mm	Actual distance between two cuts/mm	Maximum shear strength/MPa	Main location of fracture
1	83.10	9.95	5.70	3.00	2.67	403	Titanium
2	83.10	10.00	5.80	3.00	2.67	387	Titanium
3	83.10	9.95	5.80	3.00	2.85	431	Titanium
4	83.10	9.75	5.80	3.00	2.85	354	Titanium
5	83.10	9.72	5.80	3.00	2.85	401	Titanium+Interface
6	83.10	10.00	5.80	3.00	2.67	352	Titanium+Interface

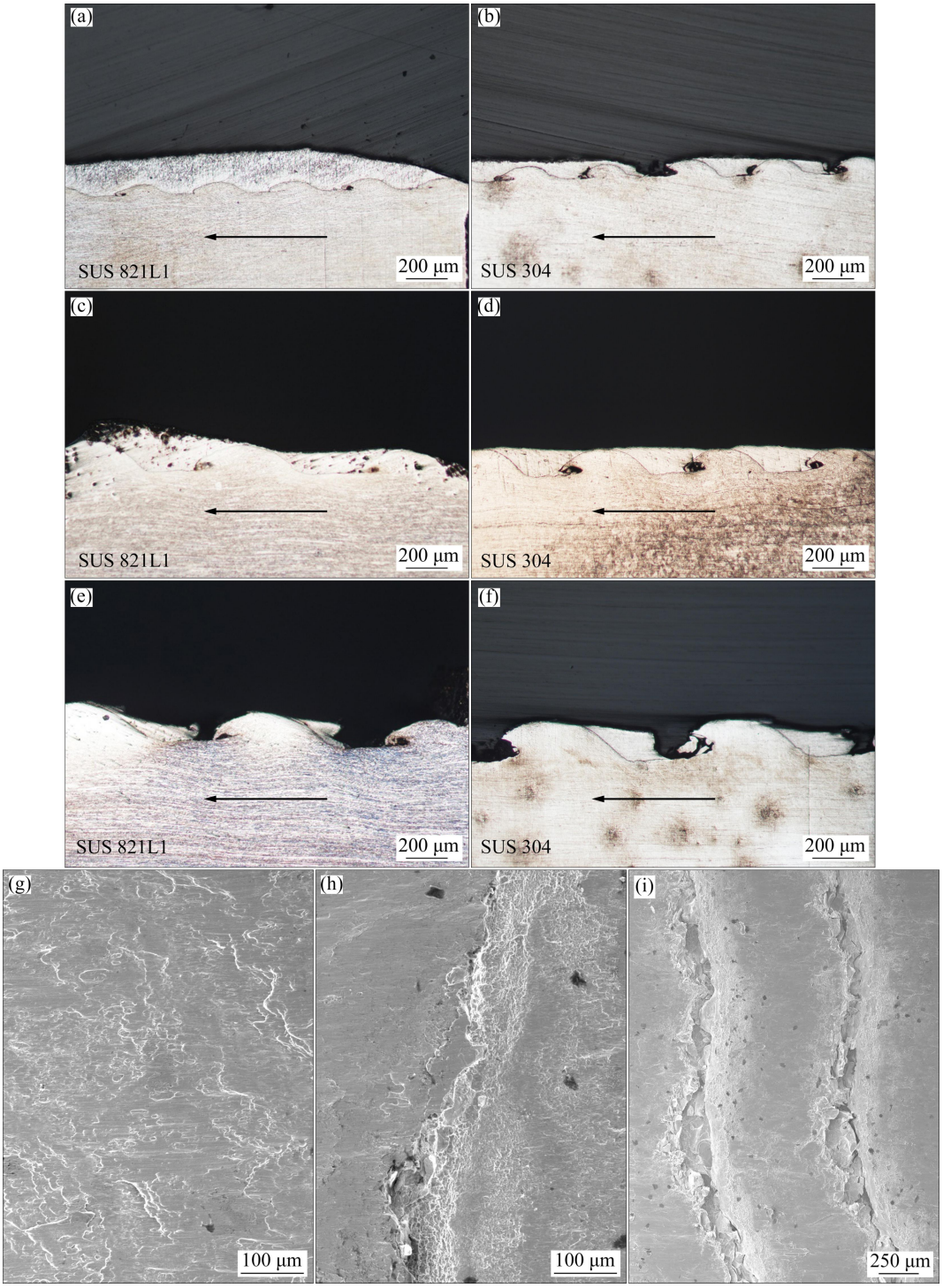

Fig. 8 Fracture morphologies: (a) Sample 1; (b) Sample 2; (c) Sample 3; (d) Sample 4; (e) Sample 5; (f) Sample 6; (g) Shear surface of Sample 1 (Ti side); (h) Shear surface of Sample 6 (Ti side); (i) Shear surface of Sample 6 (SUS 304 side)

Equation (4) gives the lower limit of the window [25], above which materials enter into a liquid state and this is necessary for the formation of a jet:

$$\beta=k\sqrt{\frac{H}{\rho V_C^2}} \tag{4}$$

where k is a constant of 0.6−1.2 and is related to surface roughness and cleanliness. H represents Vickers hardness (MPa), and ρ is the density (kg/m³). Titanium and stainless steel are difficult to weld, so k was set to be 1.0. The hardness of welding surface was used in the calculation of weldability window.

When the tensile force generated during collision leads to extensive melting at the interface, welding the materials becomes challenging. This phenomenon is referred to as the upper limit of explosive welding. Equations (5) and (6) can describe this upper limit [42]:

$$\sin\frac{\beta}{2}=\frac{K_{\mathrm{W}}}{h^{0.25}V_{\mathrm{C}}^{2}} \tag{5}$$

$$K_{\mathrm{W}}=\frac{(T_{\mathrm{m}}C_0)^{0.5}}{2N}\left(\frac{\lambda c_p C_0}{\rho}\right)^{0.25} \tag{6}$$

All the parameters in Eqs. (5) and (6) are related to the flyer plate, where β is the collision angle and h is the thickness. The parameter K_{W} is essentially dependent on the physical and thermal properties of the flyer plate, T_{m} represents the melting temperature and C_0 is the speed of sound in the bulk material. Additionally, λ represents thermal conductivity of the material while c_p is its constant pressure specific heat capacity, ρ is the density and N is a constant in the reference [43]. Under normal conditions, the value of N is 0.11 although a wider upper limit can be obtained when N is 0.037 [34]. The parameters of titanium are given in Table 5. In this study, different values of N were compared, and N=0.037 was shown to be more consistent with the experimental results.

According to research by COWAN et al [45], the Reynolds number plays an important role in the forming of a wavy interface. Therefore, they proposed Eq. (7) that can be used to calculate the critical Reynolds number (*Re*) [45]. When the *Re* is fixed, the equation can be used to calculate the critical velocity V_{c} which determines transition to the wavy interface. This is the left limit of the weldability window:

$$Re=\frac{(\rho_{\mathrm{f}}+\rho_{\mathrm{c}})V_{\mathrm{c}}^{2}}{2(H_{\mathrm{f}}+H_{\mathrm{c}})} \tag{7}$$

where ρ is the density (kg/m³) and H represents the hardness of the welding interface. The subscripts "f" and "c" refer to the flyer plate and collided plate, respectively. COWAN et al [45] experimentally obtained the critical Reynolds number of a series of metals and the values ranged from 8.1 to 13.1 with the average being 10.6. Researchers mostly use the average value in calculating the left limit [34,44], but this is usually not the case for explosive welding of titanium and stainless steel, because using 10.6 gives results that contradict the experimental findings. Notably, both COWAN et al [45] and MOUSAVI and SARTANGI [16] used 8.7 as the critical Reynolds number of cladding Ti/Steel. Therefore, the present study used an *Re* value of 8.7. The hardness of the welding interface was used in Eq. (7). Given that two types of collided plates were used in this study, two left limits were obtained. Figure 8 shows that the distance between the left limit of SUS 304 and the welding parameters was larger than that of SUS 821L1. Therefore, both the wavelength and amplitude of SUS 304 were larger.

Right limit is the sound speed limit and it is impossible to form a jet when the parameters exceed this limit. ROSSET [44] introduced a method to calculate the right limit.

The weldability window is highlighted in Fig. 9. Through the weldability window, as the collision angle increased, there was a corresponding increase in wavelength and amplitude. Based on Eq. (2), the stand-off was proportional to the collision angle in a certain range. Moreover, as the welding parameters moved to the right zone of the window, the wavelength and amplitude increased.

4 Numerical simulations

The process of explosive welding was simulated by the smoothed particle hydrodynamics (SPH) method [46]. The collision process between flyer plate and collided plate was simulated [47] and a 2D model was used, as shown in Fig. 10. The dimension of the titanium and stainless steel was 20 mm (length) × 3 mm (height), and the particle size was 10 μm. On the other hand, the dimension of steel was 60 mm (length) × 30 mm (height). The parameters used for the simulation are given in Tables 6 and 7. Given that the experimental parameters for SUS 821L1 were not available,

Table 5 Properties of titanium [44]

Density, ρ/(kg·m^{-3})	Melting temperature, T_{m}/°C	Bulk sound speed, C_0/(m·s^{-1})	Thermal conductivity, λ/(W·m^{-1}·K^{-1})	Specific heat capacity, c_p/(J·kg^{-1}·K^{-1})
4540	1660	5090	22	520

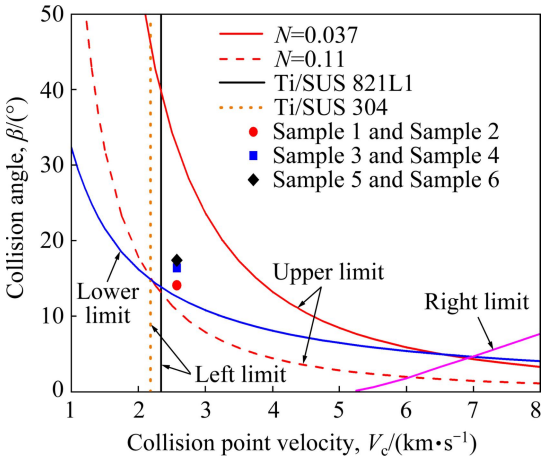

Fig. 9 Weldability window

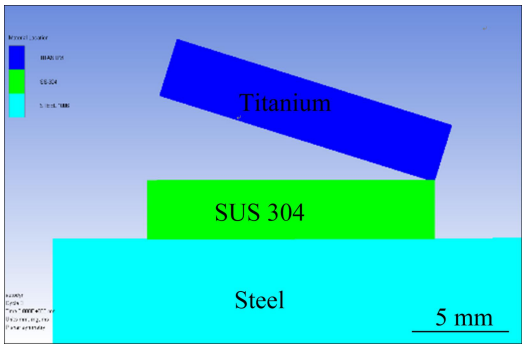

Fig. 10 Numerical model of explosive welding

those of SUS 304 were used to simulate SUS 821L1 and only the yield strength was changed to 577 MPa [18]. In this way, it was possible to study the effect of the strength of collided plate on the welding interface.

Figure 11 clearly showed that when collision velocity increased, there was corresponding increase in the amount of jet, melting (Mises stress) [50], wave and vortex zone, consistent with the experimental results. In addition, simulation revealed that the amount of jet from the titanium side was larger than that from the stainless steel side. This is because the material with a lower strength was more likely to produce a jet. Due to lack of experimental data, the parameters used in the simulation were different from the actual parameters of the material. This led to differences between the simulation results and the experimental results. However, simulation effectively predicted the trend. The simulation results showed that the higher the loss in kinetic energy loss (or stand-offs) is, the higher the wavelength and amplitude are. Besides, an increase in the strength of the collided plate led to a decrease in wavelength and amplitude, consistent with the experimental results.

Table 6 Parameters of Shock equation of state [48,49]

Material	Gruneisen coefficient, γ	Parameter C_1/(m·s^{-1})	Parameter S_1	Reference temperature/K	Specific heat capacity/(J·kg^{-1}·K^{-1})
Titanium	1.23	5020	1.536	300	520
SUS 304	2.17	4569	1.490	300	500
SUS 821L1	2.17	4569	1.490	300	500
Steel 1006	2.17	4569	1.490	300	452

Table 7 Parameters of Johnson Cook strength model [48]

Material	Density/(g·cm^{-3})	Shear modulus/kPa	Yield strength/kPa	Hardening constant/kPa	Hardening exponent
Titanium	4.528	4.4000×10^7	2.1389×10^5	3.5582×10^5	0.4381
SUS 304	7.900	8.0000×10^7	3.1000×10^5	1.0000×10^6	0.6500
SUS 821L1	7.800	8.0000×10^7	5.7700×10^5	1.0000×10^6	0.6500
Steel 1006	7.896	8.1800×10^7	3.5000×10^5	2.7500×10^5	0.3600

Material	Strain rate constant	Thermal softening	Melting temperature/K	Reference strain rate/s^{-1}	Strain rate correction
Titanium	0.02559	1.08	1941	1.0	1st order
SUS 304	0.07000	1.00	1673	1.0	1st order
SUS 821L1	0.07000	1.00	1673	1.0	1st order
Steel 1006	0.02200	1.00	1811	1.0	1st order

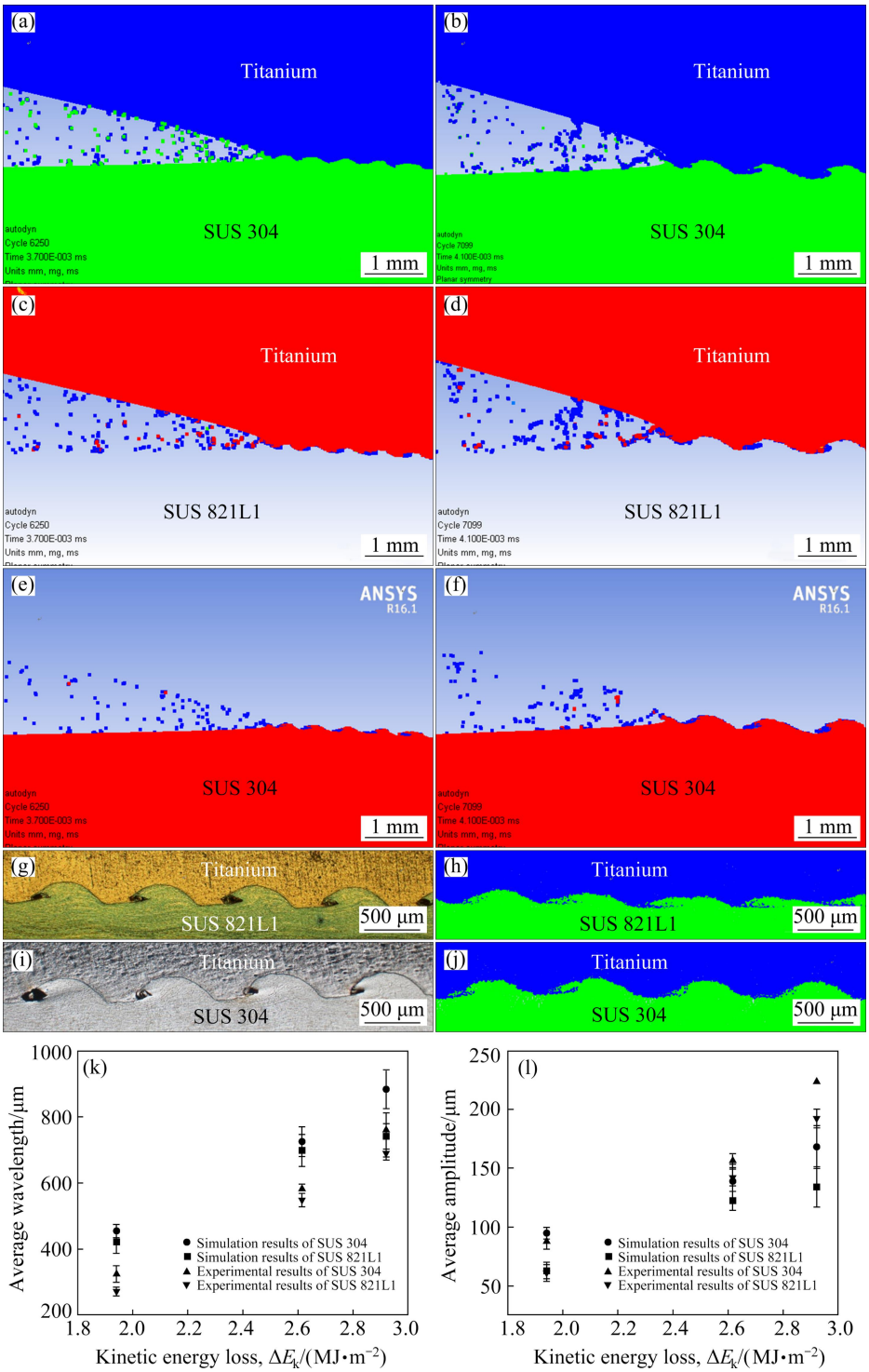

Fig. 11 Morphologies of welding interface (a−j) and comparison of simulation and experimental results (k, l): (a) Jet of 633 m/s; (b) Jet of 777 m/s; (c, e) von Mises stress of 633 m/s; (d, f) von Mises stress of 777 m/s; (g, h) Wavy and simulated interface of Sample 5; (i, j) Wavy and simulated interface of Sample 6; (k) Wavelength; (l) Amplitude

5 Conclusions

(1) Under the same welding parameters, the interface wave of SUS 821L1 was smaller than that of SUS 304. Analysis of the weldability window showed that this phenomenon occurred because the welding interface of SUS 821L1 was harder than that of SUS 304. In addition, differences in the welding results of the two types of stainless steel

were shown by the position of the adiabatic shear band. The adiabatic shear band generated in SUS 821L1 crossed the whole wave while in SUS 304 it was located at the crest of the wave.

(2) The microstructure of the vortex at the longitudinal and the transverse interfaces was observed. Additionally, the vortex region was shown to be mainly composed of titanium, chromium, iron, Fe_2Ti, Cr_2Ti and SUS 821L1. Several cracks were also identified in this region. The interface of Ti/SUS 821L11 could bear a shear load of 401−431 MPa while that of Ti/SUS 304 could withstand 352−387 MPa. Moreover, the tensile shear test results showed that when the vortex zone was small, the fracture appeared on the titanium side, indicating that the bonding strength was higher than the measured value. However, when the vortex zone increased, the fracture appeared at the interface, indicating that the measured value was the bonding strength. Therefore, a large vortex area was not good for bonding strength. Indentation test and tensile shear test indicated that the ASB can withstand a certain degree of loading.

(3) The wavy interface was simulated through the SPH method. The simulation results showed that the higher the loss in kinetic energy (or stand-offs) is, the larger the wave and vortex zone are. In addition, an increase in the strength of stainless steel led to a decrease in the wave size at the interface. The simulation results were consistent with the experimental findings. Through simulation, the jet process and melting of the interface could be obtained.

Acknowledgments

We sincerely thank Mr. M. TAKASHIMA and Mr. T. AKAIKE, Master's degree candidates, Graduate School of Science and Technology, Kumamoto University, for their help and support to conduct experiments.

References

[1] FUJI A, NORTH T H, AMEYAMA K, FUTAMATA M. Improving tensile strength and bend ductility of titanium/AlSI 304L stainless steel friction welds [J]. Materials Science and Technology, 1992, 8(3): 219−235. https://doi.org/10.1179/mst.1992.8.3.219.

[2] RAJ B, MUDALI U K. Materials development and corrosion problems in nuclear fuel reprocessing plants [J]. Progress in Nuclear Energy, 2006, 48(4): 283−313. https://doi.org/10.1016/j.pnucene.2005.07.001.

[3] LAIK A, SHIRZADI A A, SHARMA G, TEWARI R, JAYAKUMAR T, DEY G K. Microstructure and interfacial reactions during vacuum brazing of stainless steel to titanium using Ag−28%Cu alloy [J]. Metallurgical and Materials Transactions A, 2015, 46(2): 771−782. https://doi.org/10.1007/ s11661-014-2671-9.

[4] BALASUBRAMANIAN M, KUMAR R, GOPINATH S. Multi-objective optimisation of friction welding parameters in joining titanium alloy and stainless steel with a novel interlayer geometry [J]. Advances in Materials and Processing Technologies, 2020, 6(1): 25−39. https://doi.org/10.1080/2374068X.2019.1688625.

[5] ZHANG Y, ZHOU J P, SUN D Q, LI H M. Two pass laser welding of TC4 titanium alloy to 301L stainless steel via pure V interlayer [J]. Journal of Materials Research and Technology, 2020, 9(2): 1400−1404. https://doi.org/10.1016/j.jmrt. 2019.11.066.

[6] PASANG T, PRAMANA S S, KRACUM M, MISIOLEK W Z, AZIZIDEROUEI M, MIZUTANI M, KAMIYA O. Characterisation of intermetallic phases in fusion welded commercially pure titanium and stainless steel 304 [J]. Metals, 2018, 8(11): 863. https://doi.org/10.3390/met8110863.

[7] SHIRZADI A A, LAIK A, TEWARI R, ORSBORN J, DEY G K. Gallium-assisted diffusion bonding of stainless steel to titanium; microstructural evolution and bond strength [J]. Materialia, 2018, 4: 115−126. https://doi.org/10.1016/j.mtla.2018.09.009

[8] ISHIDA K, GAO Y, NAGATSUKA K, TAKAHASHI M, NAKATA K. Microstructures and mechanical properties of friction stir welded lap joints of commercially pure titanium and 304 stainless steel [J]. Journal of Alloys and Compounds, 2015, 630: 172−177. https://doi.org/10.1016/j.jallcom.2015.01.004.

[9] MANIKANDAN P, HOKAMOTO K, DERIBA A A, RAGHUKANDAN K, TOMOSHIGE R. Explosive welding of titanium/stainless steel by controlling energetic conditions [J]. Materials Transactions, 2006, 47(8): 2049−2055. https://doi.org/10.2320/matertrans.47.2049.

[10] YANG M, MA H H, SHEN Z W, CHEN D G, DENG Y X. Microstructure and mechanical properties of Al−Fe meshing bonding interfaces manufactured by explosive welding [J]. Transactions of Nonferrous Metals Society of China, 2019, 29(4): 680−691. https://doi.org/10.1016/S1003-6326(19)64978-2.

[11] RAMACHANDRAN S, LAKSHMINARAYANAN A K. An insight into microstructural heterogeneities formation between weld subregions of laser welded copper to stainless steel joints [J]. Transactions of Nonferrous Metals Society of China, 2020, 30(3): 727−745. https://doi.org/10.1016/S1003-6326(20)65249-9.

[12] MUDALI U K, RAO B M A, SHANMUGAM K, NATARAJAN R, RAJ B. Corrosion and microstructural aspects of dissimilar joints of titanium and type 304L stainless steel [J]. Journal of Nuclear Materials, 2003, 321(1): 40−48. https://doi.org/10.1016/S0022-3115(03)00194-6.

[13] KAHRAMAN N, GÜLENÇ B, FINDIK F. Joining of titanium/stainless steel by explosive welding and effect on interface [J]. Journal of Materials Processing Technology, 2005, 169(2): 127−133. https://doi.org/10.1016/j. jmatprotec. 2005.06.045.

[14] MANIKANDAN P, HOKAMOTO K, FUJITA M, RAGHUKANDAN K, TOMOSHIGE R. Control of energetic conditions by employing interlayer of different thickness for explosive welding of titanium/304 stainless steel [J]. Journal of Materials Processing Technology, 2008, 195(1−3): 232−240. https://doi.org/10.1016/j.jmatprotec. 2007.05.002.

[15] MOUSAVI S A A A, SARTANGI P F. Effect of post-weld heat treatment on the interface microstructure of explosively welded titanium–stainless steel composite [J]. Materials Science and Engineering A, 2008, 494(1−2): 329−336. https://doi.org/10.1016/j.msea.2008.04.032.

[16] MOUSAVI S A A A, SARTANGI P F. Experimental investigation of explosive welding of cp-titanium/AISI 304 stainless steel [J]. Materials & Design, 2009, 30(3): 459−468. https://doi.org/10.1016/j.matdes.2008.06.016.

[17] CHEREPANOV A N, MALI V I, MALIUTINA I N, ORISHICH A M, MALIKOV A G, DROZDOV V O. Laser welding of stainless steel to titanium using explosively welded composite inserts [J]. The International Journal of Advanced Manufacturing Technology, 2017, 90(9−12): 3037−3043. https://doi.org/10.1007/s00170-016-9657-2.

[18] MIYOSHI T. Flexural behavior of lean duplex stainless steel welded i-section [J]. Memoirs of National Institute of Technology, Akashi College, 2018, 60: 1−8.

[19] CHEN X, INAO D, TANAKA S, MORI A, Li X, HOKAMOTO, K. Explosive welding of Al alloys and high strength duplex stainless steel by controlling energetic conditions [J]. Journal of Manufacturing Processes, 2020, 58: 1318−1333. https://doi.org/10.1016/j.jmapro.2020.09.037.

[20] SUS304 stainless steel material properties, chemical composition [EB/OL]. 2021. https://www.theworldmaterial. com/sus304-stainless-steel-material/.

[21] OKADA N, TADOKORO Y, TSUGE S, GONOME F, KIZAKI M. Lean duplex stainless steel for resources saving society [J]. Zairyo-to-Kankyo, 2017, 66: 263−267. https://doi. org/10.3323/jcorr.66.263.

[22] Duplex stainless steel [EB/OL]. 2021. https://www.uex-ltd. co.jp/english/products/nisou_stainless/.

[23] NIPPON STEEL Titanium Products [EB/OL]. 2021. https://www.nipponsteel.com/product/catalog_download/pdf/ T001en.pdf.

[24] CROSSLAND B. Explosive welding of metals and its application [M]. Oxford: Clarendon Press, 1982.

[25] DERIBAS A. Science of explosive welding: State of art [C]//Proceeedings of the 4th International Symposium on Impact Engineering. Elsevier, 2001: 530−531.

[26] HOKAMOTO K, IZUMA T, FUJITA M. New explosive welding technique to weld [J]. Metallurgical Transactions A, 1993, 24(10): 2289−2297. https://doi.org/10.1007/ BF02648602.

[27] FINDIK F. Recent developments in explosive welding [J]. Materials & Design, 2011, 32(3): 1081−1093. https://doi. org/10.1016/j.matdes.2010.10.017.

[28] HUNT J N. Wave formation in explosive welding [J]. The Philosophical Magazine: A Journal of Theoretical Experimental and Applied Physics, 1968, 17(148): 669−680. https://doi.org/10.1080/14786436808223020.

[29] ZENG X Y, LI X J, CHEN X, WANG X H, YAN H H. Numerical and experimental studies on the explosive welding of plates with different initial strength [J]. Welding in the World, 2019, 63(4): 967−974. https://doi.org/10.1007/ s40194-019-00733-0.

[30] WANG L L, HU S S, YANG L M, DONG X L. Kinetics of Materials [M]. Hefei: University of Science and Technology of China Press, 2017. (in Chinese)

[31] YANG Y, WANG B F, HU B, HU K, LI Z G. The collective behavior and spacing of adiabatic shear bands in the explosive cladding plate interface [J]. Materials Science and Engineering A, 2005, 398(1−2): 291−296. https://doi.org/10. 1016/j.msea.2005.03.099.

[32] BAHRANI A S, BLACK T J, CROSSLAND B. The mechanics of wave formation in explosive welding [J]. Proceedings of the Royal Society of London. Series A: Mathematical and Physical Sciences, 1967, 296(1445): 123−136. https://doi.org/10.1098/rspa.1967.0010.

[33] GREENBERG B A, IVANOV M A, PUSHKIN M S, INOZEMTSEV A V, PATSELOV A M, TANKEYEV A P, KUZMIN S V, LYSAK, V I. Formation of intermetallic compounds during explosive welding [J]. Metallurgical and Materials Transactions A, 2016, 47(11): 5461−5473. https://doi.org/10.1007/s11661-016-3729-7.

[34] BATAEV I A, TANAKA S, ZHOU Q, LAZURENKO D V, JUNIOR A J, BATAEV A A, HOKAMOTO K, MORI A, CHEN P. Towards better understanding of explosive welding by combination of numerical simulation and experimental study [J]. Materials & Design, 2019, 169: 107649. https:// doi.org/10.1016/j.matdes.2019.107649.

[35] BATAEV I A, LAZURENKO D V, TANAKA S, HOKAMOTO K, BATAEV A A, GUO Y, JORGE JR A M. High cooling rates and metastable phases at the interfaces of explosively welded materials [J]. Acta Materialia, 2017, 135: 277−289. https://doi.org/10.1016/j.actamat.2017.06.038.

[36] KOU S. Solidification and liquation cracking issues in welding [J]. JOM, 2003, 55(6): 37−42. https://doi.org/ 10.1007/s11837-003-0137-4.

[37] ACARER M, GÜLENÇ B, FINDIK F. Investigation of explosive welding parameters and their effects on microhardness and shear strength [J]. Materials & Design, 2003, 24(8): 659−664. https://doi.org/10.1016/S0261-3069(03)00066-9.

[38] SHIRAN M R K G, BAKHTIARI H, MOUSAVI S A A A, KHALAJ G, MIRHASHEMI S M. Effect of stand-off distance on the mechanical and metallurgical properties of explosively bonded 321 austenitic stainless steel-1230 aluminum alloy tubes [J]. Materials Research, 2017, 20(2): 291−302. https://doi.org/10.1590/1980-5373-mr-2016-0516.

[39] DERIKVAND M, PANGH H. A modified method for shear strength measurement of adhesive bonds in solid wood [J]. BioResources, 2016, 11(1): 354−364.

[40] WITTMAN R. The influence of collision parameters of the strength and microstructure of an explosion welded aluminium alloy [C]//Proc 2nd Int Sym on Use of an

Explosive Energy in Manufacturing Metallic Materials. 1973: 153−168.
[41] DERIBAS A, SIMONOV V, ZAKCHARENKO I. Investigation of explosive welding parameters for arbitrary combinations of metals and alloys [C]//Proc 5th Int Conf on High Energy Rate Fabrication. University of Denver Denver, 1975: 1−4.
[42] RIBEIRO J B, MENDES R, LOUREIRO A. Review of the weldability window concept and equations for explosive welding [J]. J Phys Conf Ser, 2014, 500(5): 052038.
[43] de ROSSET W S. Analysis of explosive bonding parameters [J]. Materials and Manufacturing Processes, 2006, 21(6): 634−638. https://doi.org/10.1080/10426910600611136.
[44] Nippon steel [EB/OL]. 2021. https://en.wikipedia.org/wiki/Titanium.
[45] COWAN G R, BERGMANN O R, HOLTZMAN A H. Mechanism of bond zone wave formation in explosion-clad metals [J]. Metallurgical and Materials Transactions B, 1971, 2(11): 3145−3155. https://doi.org/10.1007/BF02814967.
[46] LIU M B, LIU G R. Smoothed particle hydrodynamics (SPH): An overview and recent developments [J]. Archives of Computational Methods in Engineering, 2010, 17(1): 25−76. https://doi.org/10.1007/s11831-010-9040-7.
[47] LI X J, MO F, WANG X H, WANG B, LIU K X. Numerical study on mechanism of explosive welding [J]. Science and Technology of Welding and Joining, 2012, 17(1): 36−41. https://doi.org/10.1179/1362171811Y.0000000071.
[48] JOHNSON G, COOK W. Selected hugoniots: EOS [C]//7th International Symposium on Ballistics. 1969: LA-4167-MS.
[49] CHANG L, ZHOU C Y, PENG J, LI J, HE X H. Fields–Backofen and a modified Johnson-Cook model for CP-Ti at ambient and intermediate temperature [J]. Rare Metal Materials and Engineering, 2017, 46(7): 1803−1809. https://doi.org/10. 1016/S1875-5372(17)30170-4.
[50] CHEN X, LI X J, WANG X H, YAN H H, LI K B, ZENG X Y. Bonding mechanism of explosive compaction–welding sintering [J]. Journal of Manufacturing Processes, 2019, 46: 1−15. https:// doi.org/10.1016/j.jmapro.2019.08.018.

爆炸焊接 Ti/SUS 304 与 Ti/SUS 821L1 的对比

陈 翔[1]，Daisuke INAO[2]，Shigeru TANAKA[1]，李晓杰[3]，I. A. BATAEV[4]，Kazuyuki HOKAMOTO[1]

1. Institute of Industrial Nanomaterials, Kumamoto University, 860-8555 Kumamoto, Japan;
2. Faculty of Engineering, Kumamoto University, 860-8555 Kumamoto, Japan;
3. 大连理工大学 工业装备结构分析国家重点实验室和工程力学系，大连 116024；
4. Faculty of Mechanical Engineering and Technologies,
Novosibirsk State Technical University, K. Marks 20, 630073 Novosibirsk, Russia

摘 要：将商业纯钛分别与 SUS 304 奥氏体不锈钢和 SUS 821L1 双相不锈钢进行焊接。得到的 Ti/SUS 821L1 的波状界面小于 Ti/SUS 304 的。从纵向和横向均可观察到涡旋区域，并对涡旋区域的成分进行分析。Ti/SUS 821L1 的界面可以承受 401~431 MPa 的剪切载荷，Ti/SUS 304 的界面可以承受 352~387 MPa 的剪切载荷。使用爆炸焊接窗口来解释实验现象。使用光滑粒子动力学对波状界面进行数值模拟，模拟得出的波长与波幅随不锈钢强度与炸高的变化趋势与实验结果相符合。

关键词：爆炸焊接；钛；双向不锈钢；拉伸剪切测试；焊接窗口；光谱粒子动力学(SPH)

(Edited by Bing YANG)